THE JOURNAL OF BIOLOGICAL CHEMISTRY VOL. 284, NO. 19, pp. 13119–13127, May 8, 2009

lin9 Is Required for Mitosis and Cell Survival during Early Zebrafish Development*[S]

Received for publication, December 22, 2008, and in revised form, February 10, 2009 Published, JBC Papers in Press, March 11, 2009, DOI 10.1074/jbc.M809635200

Markus A. Kleinschmidt[‡], Toni U. Wagner[‡], Daniel Liedtke[‡], Susi Spahr[‡], Birgit Samans[§], and Stefan Gaubatz[‡1]

From the [‡]Department of Physiological Chemistry I, Biocenter, University of Wuerzburg, Am Hubland, 97074 Wuerzburg and the [§]Institute of Molecular Biology and Tumor Research, Philipps-University of Marburg, Emil-Mannkopff-Strasse 2, 35032 Marburg, Germany

LIN9 has been described as a regulator of G_1/S and G_2/M progression of the cell cycle in invertebrates and human cell lines. To elucidate the *in vivo* function of LIN9 during vertebrate development, we took advantage of the teleost zebrafish (*Danio rerio*). By means of antisense morpholinos we show here that Lin9-depleted embryonic cells accumulate in mitosis. Flow cytometry and confocal microscopy data demonstrate that the delay in mitotic progression is followed by apoptosis, which strongly manifests in the developing central nervous system. In accordance with these findings, we identified a cohort of Lin9-regulated genes required for different mitotic processes, including mitotic entry, metaphase/anaphase transition, and cytokinesis. Our data establish LIN9 as an essential regulator of mitosis in vertebrate development.

The transition from G_1 to S phase marks the starting point of the eukaryotic cell to replicate its chromosomal set of DNA. This event is followed by the G_2 period that prepares the cell for mitosis, a process that results in the separation of the duplicate chromosome set into two nuclei. The progression through the cell cycle is regulated by multiple processes, including regulated gene transcription. For example, E2F transcription factors play a key role in the activation of S phase entry genes during the G_1 phase of the cell cycle (reviewed in Ref. 1). Likewise, several transcription factors are implicated to play a role in the activation of mitotic genes during S phase, among them NF-Y, B-MYB, and FOXM1 (2–4).

LINC/DREAM is a recently identified multiprotein complex that is required for two transcriptional processes that act on cell cycle regulation, namely repression of genes that drive G_1/S transition and activation of genes required for G_2/M progression (3, 5, 6). LINC/DREAM consists of the core members LIN9, LIN54, LIN37, LIN52, and RBAP48. Interestingly, LINC/DREAM undergoes a dynamic and cell cycle-dependent switch of subunits (7, 8). In G_0/G_1, the complex is associated with p130 and E2F4, whereas in late S phase it interacts with B-MYB and activates G_2/M promoters.

* This work was supported by Deutsche Forschungsgemeinschaft Grant TR 17 (to S. G. and D. L.) and a European Union grant (Plurigenes FP6 project 018673) (to T. W.).

[S] The on-line version of this article (available at http://www.jbc.org) contains supplemental Figs. 1–4.

[1] To whom correspondence should be addressed: Dept. of Physiological Chemistry I, Biocenter, University of Wuerzburg, Am Hubland, 97074 Wuerzburg, Germany. Tel.: 49-931-3184138; E-mail: stefan.gaubatz@biozentrum.uni-wuerzburg.de.

LINC/DREAM is evolutionarily highly conserved. A DREAM-like complex was first purified from *Drosophila* embryo lysates and was named Myb-MuvB (MMB) or dREAM (for *Drosophila* RBF-, dE2F2-, and dMyb-interacting proteins) (9, 10). Although initially described as complexes involved in the repression of E2F target genes during fly development, a recent study indicates that dREAM/Myb-MuvB also regulate the activation of genes required for mitotic progression (11). Furthermore, a related complex has also been identified in *Caenorhabditis elegans* (12).

B-MYB, a subunit of the activating LINC complex in S phase and G_2, is essential for early mouse embryogenesis, and its short hairpin RNA-mediated knockdown in murine ES cells results in a delay of G_2/M progression, mitotic spindle and centrosome defects, and polyploidy (13, 14). In zebrafish, the *bmyb* loss-of-function mutation *crash&burn* (*crb*) results in a similar phenotype. *crb* fish exhibit defects in spindle formation and show genomic instability (15). *crb* embryonic cells accumulate in G_2/M, and down-regulation of cyclin B is at least in part causative for this delay in cell cycle progression.

We and others have shown that LIN9, a core subunit of LINC, activates G_2/M genes in human cells together with B-MYB. Mice carrying an 84-amino acid N-terminal deletion LIN9 have recently been generated (16). However, except for a mild increase in body size, they do not show any obvious phenotype. Since highly conserved regions of LIN9 are still retained, it is unlikely that Δ84 LIN9 represents a complete loss-of-function protein. Thus, the role of LIN9 in vertebrate development is still unclear.

To address the role of LIN9 in vertebrate development we now used zebrafish as a model system. We found that *lin9* is essential for early zebrafish development. The loss of *lin9* leads to an accumulation of embryonic cells in mitosis and an increase of apoptosis. Genome-wide gene expression analysis shows that Lin9 regulates a cluster of genes required for mitotic processes, among them the G_2/M and the spindle assembly checkpoint, chromosome segregation, and cytokinesis. Our data suggest an overlap of B-MYB and LIN9 function throughout vertebrate development and establish the latter as a critical regulator of mitotic progression.

EXPERIMENTAL PROCEDURES

Morpholino and mRNA Injections—TÜAB zebrafish were maintained and staged as described (17, 18). The indicated

times refer to hours postfertilization (hpf)[2] at 28.5 °C. Embryos were kept in 1× Danieau solution (58 mM NaCl, 0.7 mM KCl, 0.4 mM $MgSO_4$, 0.6 mM $Ca(NO_3)_2$, 5 mM HEPES, pH 7.6, 0.0001% methylene blue). Morpholinos (Gene Tools, Philomath, OR) were designed against *Danio rerio lin9* homolog (GenBank™ accession NM_001044946). The morpholino (MO) sequences were as follows: MO-ATG, 5′-CTCGAGCTCCGCCATCTTGAATTAG-3′; MO-E1, 5′-GTTAGTTTTATTACTCACTCTCGTC-3′; 5-base mismatch morpholino MO-E1mis, 5′-GTTACTTTTAATACTGACTGTCCTC-3′. The indicated amounts of morpholinos were injected into one- or two-cell stage embryos. To follow morpholino uptake, a small amount (3.5 pmol) of fluorescein isothiocyanate-dextran (Sigma) was cooinjected. For capped RNA synthesis, plasmids containing full-length cDNAs for *lin9* and *ccnb1* (clone IRBOp991B0331D, obtained from imaGenes (Berlin, Germany)) were used. Linearized plasmids were transcribed *in vitro* with SP6 RNA polymerase using the mMessage mMachine kit from Ambion (Austin, TX).

RNA Isolation, Reverse Transcription (RT), PCR, and Cloning—20 embryos were dechorionated, washed in PBS, transferred to a 2 ml tube and homogenized in RLT buffer (Qiagen) with a micropestle. Total RNA was purified by means of an RNeasy minikit (Qiagen) according to the manufacturer's protocol. 0.65 μg of RNA were applied to RT by incubation with 0.5 μg of oligo$(dT)_{17}$ primer and 100 units of Moloney murine leukemia virus reverse transcriptase (Promega) in a total volume of 25 μl. For end point PCR, we used the following primers: *ef1a* (NM_131263, bases 415–969), forward (5′-TGATTGTTGCTGGTGGTGTT-3′) and reverse (5′-GAGACTCGTGGTGCATCTCA-3′); *lin54* (NM_001076567, bases 2037–2392), forward (5′-AGGCTGCAACTGCAAGAAAT-3′) and reverse (5′-CCTGCGGTTGATTGGTAAGT-3′); *bmyb* (NM_001003867, bases 797–1185), forward (5′-AGAACTGCCTGTCGAATGCT-3′) and reverse (5′-GACTCAGGATGGATGGAGGA-3′); *lin9* (NM_001044946, bases 502–1043), forward (5′-AGTTGACCCGAGTTGAATGG-3′) and reverse (5′-CAGAGTCTCTCCGTCGGTTC-3′). For whole mount *in situ* hybridizations, the PCR product generated with the last pair of primers was TA-cloned into pCRII (Invitrogen). Clones were obtained with inserts in sense and antisense orientation. For amplification of full-length zebrafish *lin9*, we used the following primers: forward, 5′-TTTTGGATCCATGGCGGAGCTCGAGCAGCT-3′; reverse, 5′-TTTGCGGCCGCTCACGTTCTGTTGGTGTTGTTT-3′. The PCR product was cloned into pcDNA3 via BamHI and NotI restriction sites. Sequencing revealed that *lin9* cDNA differed from GenBank™ accession number NM_001044946 in bases 155 (G to T) and 434 (T to A), resulting in an alteration of amino acid residue 39 (Gln to His). Quantitative PCR was performed using ABsolute™ QPCR SYBR Green Mix (ThermoScientific, Epsom, UK) and the Mx3000P real time detection system (Stratagene, La Jolla, CA) using the following primers: *actb* (NM_131031, bases 10–100), forward (5′-GATCTTCACTCCCCTTGTTCA-3′) and reverse (5′-ATACCGGAGCCGTTGTCA-3′); *pif1* (NM_198807, bases 1697–1774), forward (5′-GCAGCTGCCACTCAAACTG-3′) and reverse (5′-GAGATCTCCACACAATCCAGAGT-3′); *aspm* (ENSDART00000105631, bases 1697–1774), forward (5′-GCCCTTAAATCAGCCAAGAA-3′) and reverse (5′-TTCTCTGCAGTTTTGCCCTAA-3′); *top2a* (NM_001003834, bases 2961–3034), forward (5′-CACCACCATCGAGATCACAG-3′) and reverse (5′-CCAACACATTCTCCTTATAGGTCA-3′); *cdc20* (NM_213080, bases 1317–1389), forward (5′-AATGCTTCCAGTGGCTCTTG-3′) and reverse (5′-TGGGTGCAAAAACAAGAGAAG-3′); *oip5* (XM_001339446, bases 260–335), forward (5′-GACTCTCTCGGCGTCTGC-3′) and reverse (5′-CCATCACATCCTCAGTAACTTTCA-3′); *bax* (NM_131562, bases 312–418), forward (5′-GCCCGTGAGATCTTCTCTGA-3′) and reverse (5′-TCAGGAACCCTGGTTGAAAT-3′); *tnfb* (NM_001024447, bases 238–312), forward (5′-GGTCAGAAACCCAACAGAGAA-3′) and reverse (5′-CACTTTTCCGTGGTCTGAGG-3′). Triplicate mean values were calculated according to the *ct* quantification method using the *actb* transcript level as reference for normalization (19).

Whole Mount in Situ Hybridization—pCRII-*lin9* vectors (see "RNA Isolation, Reverse Transcription (RT), PCR, and Cloning") were linearized with XhoI. *pif1* (NM_198807, bases 168–810), *aspm* (ENSDART00000105631, bases 621–1370), *top2a* (NM_001003834, bases 3785–4401), and *oip5* (XM_001339446, bases 40–646) templates were amplified from cDNA with reverse primers providing the SP6 promoter sequence. *In vitro* transcription was performed using SP6 polymerase and the DIG RNA labeling kit (Roche Applied Science), according to the manufacturer's instructions. Whole mount *in situ* hybridization was carried out as previously described (17). Nitro blue tetrazolium/bromo-4-chloro-3-indolyl phosphate (Roche Applied Science) served as a substrate for color development.

Flow Cytometry—Upon removal of the chorion, 10 embryos were washed in PBS and transferred to a collection tube. Embryos were homogenized with a micropestle in Dulbecco's modified Eagle's medium + 10% fetal calf serum at 4 °C, passed through a 30-μm filter (Beckman Coulter), collected in a 15-ml tube, and centrifuged at 1200 rpm at 4 °C. Cells were washed once in PBS and stained in DNA buffer (100 mM Tris, pH 7.5, 154 mM NaCl, 1 mM CaCl, 0.5 mM MgCl, 0.2% bovine serum albumin, 0.1% Nonidet P-40, 250 μg/ml RNase, 30 μg/ml propidium iodide) for at least 30 min at 4 °C in the dark. DNA content was analyzed with a Cytomics FC 500 (Beckman Coulter) flow cytometer.

Apoptosis Detection—72-h zebrafish embryos were incubated for 30 min in 5 μg/ml acridine orange in PBS and subsequently washed twice for 20 min in PBS at room temperature. For microscopic examination embryos were transferred into ice-cold PBS, 0.01% 3-aminobenzoic acid ethyl ester methane sulfonate. Terminal transferase-mediated dUTP nick end-labeling (TUNEL) assays were performed as described elsewhere (20).

Confocal Microscopy—Embryos were fixed and prepared as described previously (21). For DNA staining, embryos were incubated in 10 μg/ml Hoechst (PBS) for 30 min. For imaging, Leica

[2] The abbreviations used are: hpf, hours postfertilization; MO, morpholino; RT, reverse transcription; PBS, phosphate-buffered saline; TUNEL, terminal transferase-mediated dUTP nick end-labeling; qPCR, quantitative PCR.

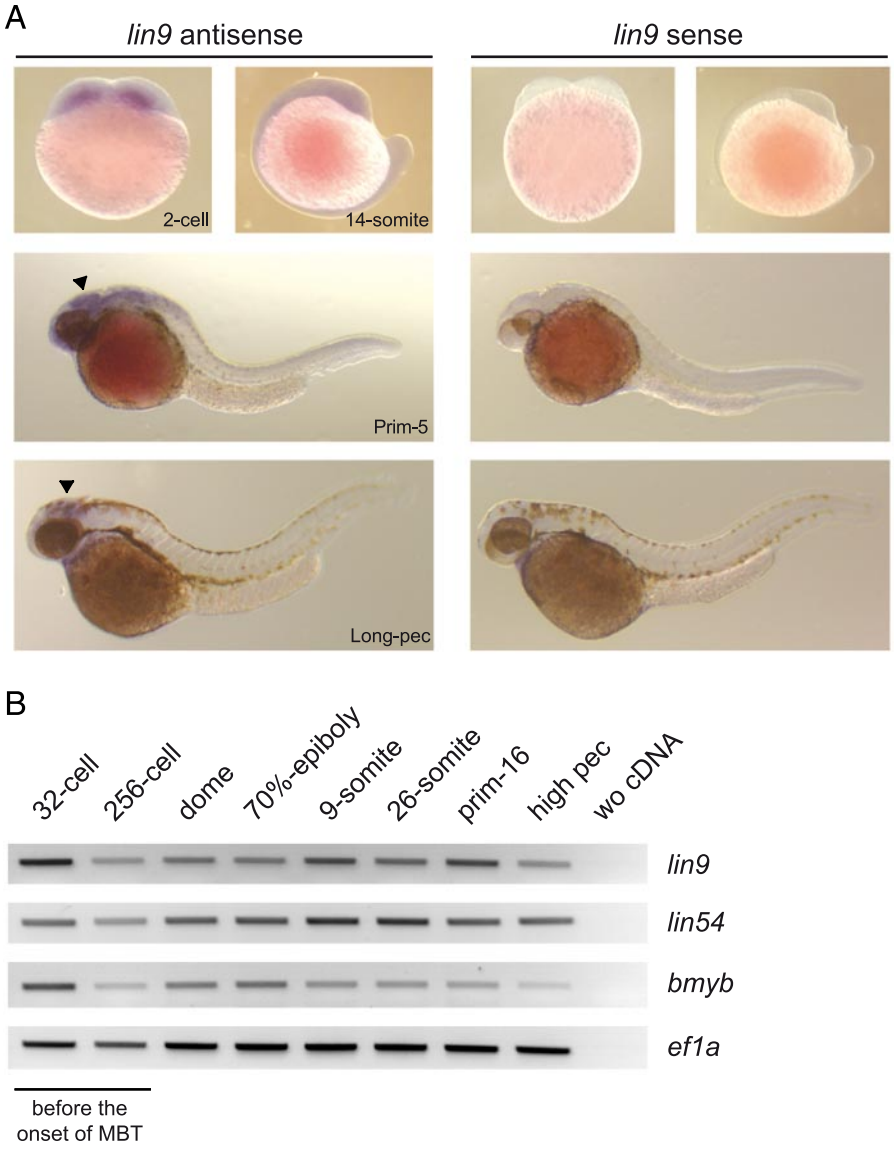

FIGURE 1. ***lin9* is expressed throughout zebrafish development.** *A*, whole mount *in situ* hybridization was carried out at the indicated hpf with an antisense and sense probe for *lin9*. *Arrowheads* mark the optic tectum. *B*, semiquantitative RT-PCR at the indicated stages reveals that *lin9*, *lin54*, and *bmyb* transcripts are present during embryogenesis before and after the midblastula transition (*MBT*).

(Wetzlar, Germany) SP2 and SP5 inverted confocal systems were used. The resulting multidimensional stacks were analyzed using ImageJ version 1.41 (National Institutes of Health) and Volocity 4/5 (Improvision, Coventry, UK) software.

Gene Expression Analysis—20 embryos/condition (MO-E1; MO-E1mis) were pooled for RNA purification 24 h postfertilization. Using the two-color Quick-Amp Labeling Kit (catalog number 5190-0444; Agilent), 100 ng of total RNA were used for cDNA synthesis, mRNA amplification, and labeling according to the manufacturer's instructions. Transcriptional profiling was done on a zebrafish oligonucleotide array (catalog number G2519F AMADID 019161; Agilent) in a 4 × 44,000 slide format and analyzed as described before (22). Expression data and gene annotations were stored in Array Express (available on the World Wide Web) (accession number A-MEXP-1510), which complies with MIAME (minimal information about a microarray experiment) guidelines. For experimental comparisons, genes showing at least a 1.6-fold change were chosen.

RESULTS

lin9 Is Expressed throughout Zebrafish Embryonic Development—To analyze *lin9* expression in zebrafish embryogenesis, we performed whole mount *in situ* hybridization on paraformaldehyde-fixed embryos at 0.45, 16, 32, and 48 h postfertilization (2-cell, 14-somite, Prim-16, and Long-pec stage, respectively). The probe was designed targeting bases 502–1043 of *lin9* mRNA (NM_001044946). Blast analysis, even under lowest stringency conditions, did not reveal any target other than *lin9*. Transcripts of *lin9* were detected throughout embryogenesis. Expression was ubiquitous at the first embryonic day and became restricted to the head region, most notably to the optic tectum of the mesencephalon at later stages of development (Fig. 1*A*). Because the *lin9* message is already present at the two-cell stage and because zebrafish zygotic transcription arises at the midblastula transition (1000-cell stage), these data indicate that *lin9* is a maternally derived transcript. We independently confirmed these results by RT-PCR analysis (Fig. 1*B*). Other members of the LINC complex, namely *lin54* and *bmyb*, are also expressed during early zebrafish embryogenesis (Fig. 1*B*).

lin9 Is Essential for Early Zebrafish Development—To analyze the role of *lin9* in early zebrafish development, we designed an antisense MO that targets the splice donor site of exon 1 of the *lin9* transcript (MO-E1; Fig. 2*A*). To confirm that MO-E1 indeed inhibits the correct splicing of the *lin9* message, we microinjected 7 ng of MO-E1 into the yolk of one- or two-cell stage embryos and analyzed the *lin9* message by semiquantitative RT-PCR 3 days later. As shown in Fig. 2*B*, the band corresponding to the spliced *lin9* message is strongly reduced upon injection of MO-E1. In addition, a shorter message that arises from the use of a cryptic splice site can be detected in MO-E1-injected zebrafish embryos. We further confirmed both PCR products by sequencing. A schematic representation of the cryptic variant is depicted in supplemental Fig. 1.

Next, we microinjected embryos with MO-E1 and followed their development. In order to exclude off-target or secondary

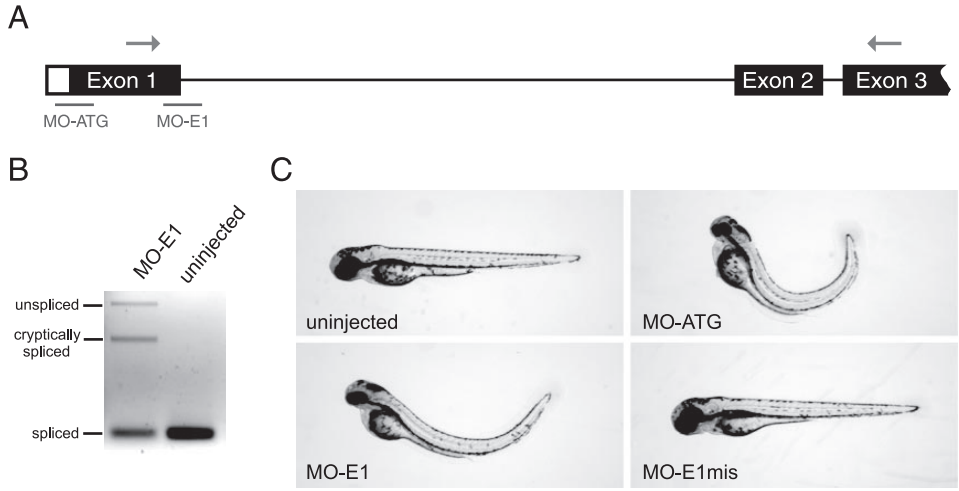

FIGURE 2. ***lin9* is essential for zebrafish development.** *A*, schematic representation of the unspliced *lin9* transcript. Morpholino targeting sites (*lines*) and binding sites for PCR primer (*arrows*) are indicated. *B*, injection of MO-E1 (7 ng) prevents splicing of intron 1 or results in a cryptic splice variant. Semiquantitative RT-PCR was conducted 72 hpf. *C*, *lin9* morphants display small head and eyes, cardiac edema, and trunk curvature. A 5-base mismatch morpholino (MO-E1mis) did not evoke developmental defects. Images were taken 72 hpf.

TABLE 1
Summary of mopholino and mRNA injections

Morpholino	Amount	mRNA	*n*	s.h.[a] (+curvature)	WT[b]	Percentage of WT
	ng					*%*
ATG	15		120	116	4	3.3
ATG	7		87	43	44	50.6
E1	15		99	97	2	2.0
E1	7		78	69	9	11.5
E1	3.4		104	73	28	26.9
E1	3.4	LIN9 (0.2 ng)	50	23	27	54
E1mis	15		100	1 (+3)	96	96
E1mis	7		68	0 (+1)	67	98.5

[a] Small head.
[b] WT, wild type.

effects, we included a control morpholino (MO-E1mis) in our experiments. MO-E1mis differs from the E1 morpholino in 5 bases (see "Experimental Procedures"). MO-E1mis-injected embryos developed virtually identically compared with uninjected wild type embryos. In stark contrast, at day 2 of development, MO-E1-injected zebrafish embryos (morphants) had slightly smaller heads than uninjected or control-injected embryos. At day 3, in almost all *lin9* morphants, a stronger phenotype was evident. Specifically, ME-E1-injected embryos had a small head, small eyes, pericardial edema, and a strong trunk curvature (Fig. 2*C*). When we tested various amounts of MO-E1, we found that 3.4 ng was sufficient to induce the morphant phenotype in 73.1% of all embryos (Table 1). Higher doses of the morpholino increased the fraction of zebrafish with the morphant phenotype but did not alter the phenotype. Importantly, however, when embryos were coinjected with 3.4 ng of MO-E1 and 0.2 ng of *in vitro* transcribed *lin9* mRNA, only 46% of the embryos showed the morphant phenotype, strongly suggesting that the phenotype arises due to the inhibition of *lin9* expression. Injection of *lin9* mRNA alone did not result in phenotypical alterations (data not shown). Furthermore, a second *lin9*-specific morpholino (MO-ATG) that is predicted to interfere with the translation of the *lin9* message showed the same phenotype as MO-E1 (Fig. 2*C*). Since two morpholinos targeting *lin9* induced the same phenotype and since this phenotype was partially rescued by the *lin9* mRNA, we conclude that the morphant phenotype is due to the loss of Lin9.

Lin9 Regulates the Embryonic Cell Cycle—Next, we analyzed the embryonic cell cycles of *lin9* morphant embryos by flow cytometry 30 and 48 h after fertilization. Injection of both *lin9*-specific morpholinos, but not MO-E1mis, resulted in a decrease of cells in G_1 and an increase of cells with a G_2/M DNA content (Fig. 3*A*). In addition, a large number of cells with a sub-G_1 DNA content were detected in *lin9* morphants, suggesting that cells undergo apoptosis or necrosis upon loss of Lin9. Taken together, these results demonstrate that loss of Lin9 leads to an accumulation of cells in G_2/M and an increase of cell death during zebrafish embryogenesis.

Apoptosis and Accumulation of Mitotic Cells in lin9 Morphant Brains—The number of cells with a sub-G_1 DNA content strongly increased in *lin9* morphants between 24 and 48 h after fertilization (Fig. 4*C*). To further analyze cell death in *lin9* morphants, we used acridine orange to visualize apoptotic areas under the fluorescence microscope in 72-h-old zebrafish embryos. As shown in Fig. 4*A*, the olfactory regions of uninjected and control injected (E1mis) embryos were stained by acridine orange, indicating physiologically occurring apoptosis (23). Strikingly, in *lin9* morphant brains, fluorescence-positive areas were much more widely distributed compared with control embryos, suggesting massive apoptosis in the developing brain upon loss of Lin9. To independently confirm apoptosis in the morphants, we made use of the TUNEL assay (Fig. 4*B*). These experiments confirmed enhanced apoptosis in the heads of 48 h morphants, most strikingly in the central nervous system and olfactory region.

To further substantiate this observation, we took confocal images of Hoechst-stained embryonic nuclei 30 h after fertilization. We noticed a plethora of apoptotic bodies in brains of *lin9* morphant embryos but not in control embryos. Overall, about 20% of all nuclei showed an abnormal morphology, including nuclear shrinkage and fragmentation, which are known features of programmed cell death (Fig. 5, *bottom*). Second, quantification revealed a more than 3-fold higher number of mitotic cells in the developing brain of morphant embryos compared with uninjected embryos. This suggests that the increase in the fraction of cells in G_2/M observed by fluorescence-activated cell sorting analysis is, at least in part, due to accumulation of cells in mitosis. Importantly, the increase in apoptotic and mitotic cells was also observed in the developing brains of zebrafish embryos injected with MO-ATG (supplemental Fig. 2). Taken together, these findings indicate that

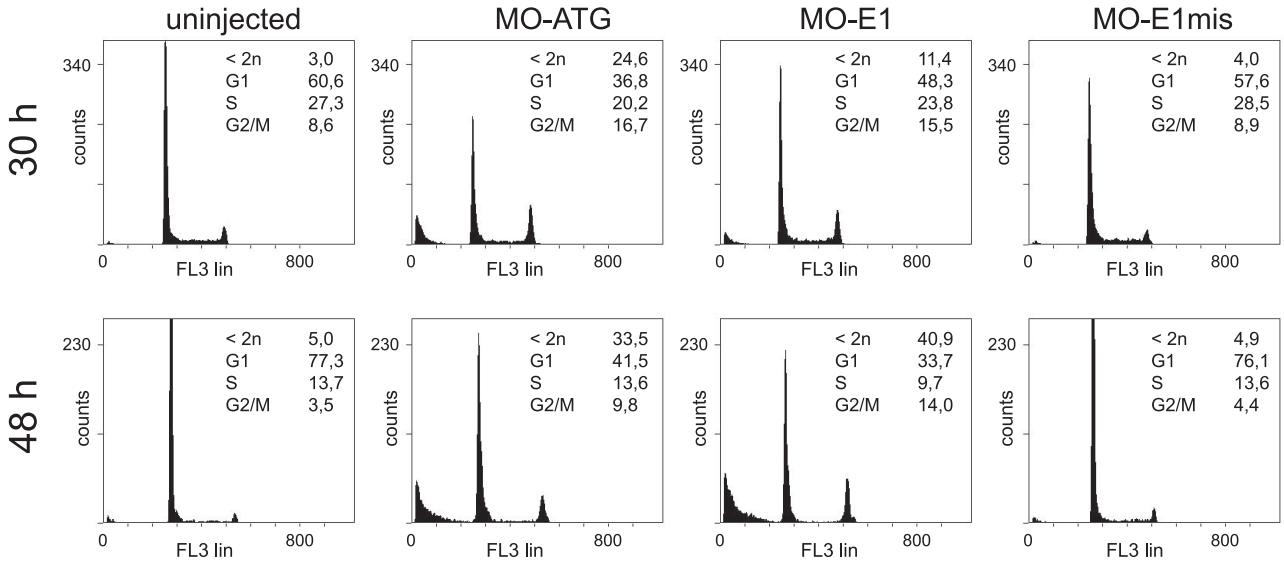

FIGURE 3. **Cell death and G_2/M delay in *lin9* morphants.** Embryos were injected with 7 ng of indicated morpholinos. At 30 and 48 hpf, clutches of 10 embryos were homogenized. For DNA content analysis, cells were stained with propidium iodide and analyzed by flow cytometry. MO-ATG and MO-E1 evoke an increase of cell number in G_2/M 30 hpf compared with uninjected or control (MO-E1mis)-injected embryos. The amount of dead cells (*<2n*) increases from 30 to 48 hpf in the morphants.

developing cells in the zebrafish brain undergo apoptosis upon loss of Lin9, possibly preceded by mitotic defects.

Lin9 Regulates a Cohort of Genes Required for Mitosis—Because in human cells, LIN9 regulates the expression of genes that are required for entry into mitosis, including cyclin B1 (3, 6), we next asked whether inhibition of cyclin B1 is responsible for the observed phenotype. To address this possibility, we first analyzed the expression of cyclin B1 in *lin9* morphants by RT-qPCR. Cyclin B1 was indeed slightly down-regulated in MO-ATG as well as in MO-E1 morphant embryos (Fig. 6*A*). Next, we asked whether cyclin B1 expression can restore a normal cell cycle profile in *lin9* morphants. To address this question, we coinjected MO-E1 with *in vitro* transcribed cyclin B1 mRNA. As a positive control, we coinjected MO-E1 with *lin9* mRNA. As expected, *lin9* mRNA greatly reduced both cell death and G_2/M accumulation when coinjected with MO E1 (Fig. 6*B*). However, cyclin B1 mRNA neither rescued the accumulation of cells in G_2/M nor prevented the apoptosis upon injection of MO-E1. These observations indicate that inhibition of cyclin B1 is not sufficient to explain the *lin9* morphant phenotype. Therefore, we performed genome-wide gene expression analysis using a zebrafish oligonucleotide microarray to identify genes regulated by Lin9 during zebrafish development. We compared gene expression profiles of morphant (E1) and control-injected (E1mis) embryos 24 h after fertilization, a time when cell cycle defects first become detectable by flow cytometry (data not shown). The microarray analysis identified 109 genes that were down-regulated and 49 genes that were up-regulated more than 1.6-fold in the *lin9* morphants (Fig. 7 and supplemental Fig. 3). Interestingly, although genes required for the G_1/S transition were not affected by the inhibition of Lin9, at least 25% of the down-regulated genes function in mitosis (Fig. 7*A* and supplemental Fig. 3). These genes encode for proteins required for entry into mitosis, spindle assembly, centrosome formation, metaphase/anaphase transition, and cytokinesis (Fig. 7*B*).

We next used RT-qPCR to validate regulation of selected genes identified in the microarray experiment (Fig. 7*C*). As a control, we also included cDNA from uninjected and MO-ATG-injected embryos. The expression levels of all genes tested, including *pif1*, *aspm*, *top2a*, and *oip5*, were down-regulated in both MO-E1 and MO-ATG morphant zebrafish compared with control injected (E1mis) and uninjected embryos. To independently confirm these results, we performed whole mount *in situ* hybridization on 24 h MO-E1- and MO-E1mis-injected embryos with probes directed at *pif1*, *aspm*, *top2a*, and *oip5* (Fig. 7*D*). As expected, MO-E1-injected embryos displayed a weaker signal for all probes compared with MO-E1mis embryos. These results together with the findings presented above support a role for Lin9 in the regulation of mitotic progression during zebrafish development.

Although we detected enhanced apoptosis in Lin9-deficient embryos (Figs. 4 and 5), we did not detect a significant enrichment of apoptosis-related genes in the microarray experiment. However, one apoptosis-related gene up-regulated in *lin9* morphants is *tnfb* (supplemental Fig. 3). Tnfb is a member of the tumor necrosis factor superfamily and shows 51% similarity with human LTA/TNFB. RT-qPCR showed that *tnfb* is up-regulated at least 1.7-fold in both MO-E1- and MO-ATG-injected embryos. We also analyzed the expression of *bax*, a proapoptotic and *bona fide* p53 target gene (supplemental Fig. 4). In contrast to *tnfb*, *bax* expression was unaltered in *lin9* morphants.

DISCUSSION

Here, we made use of the zebrafish as a vertebrate model, whose rapid embryogenesis *ex utero* allowed us to study the *in vivo* function of *lin9* by morpholino injection. Loss of Lin9 causes an increase of cell number in mitosis, which is most likely ascribed to the down-regulation of a cohort of mitotic genes we identified by gene expression analysis. LIN9-dependent genes regulate different mitotic processes. For

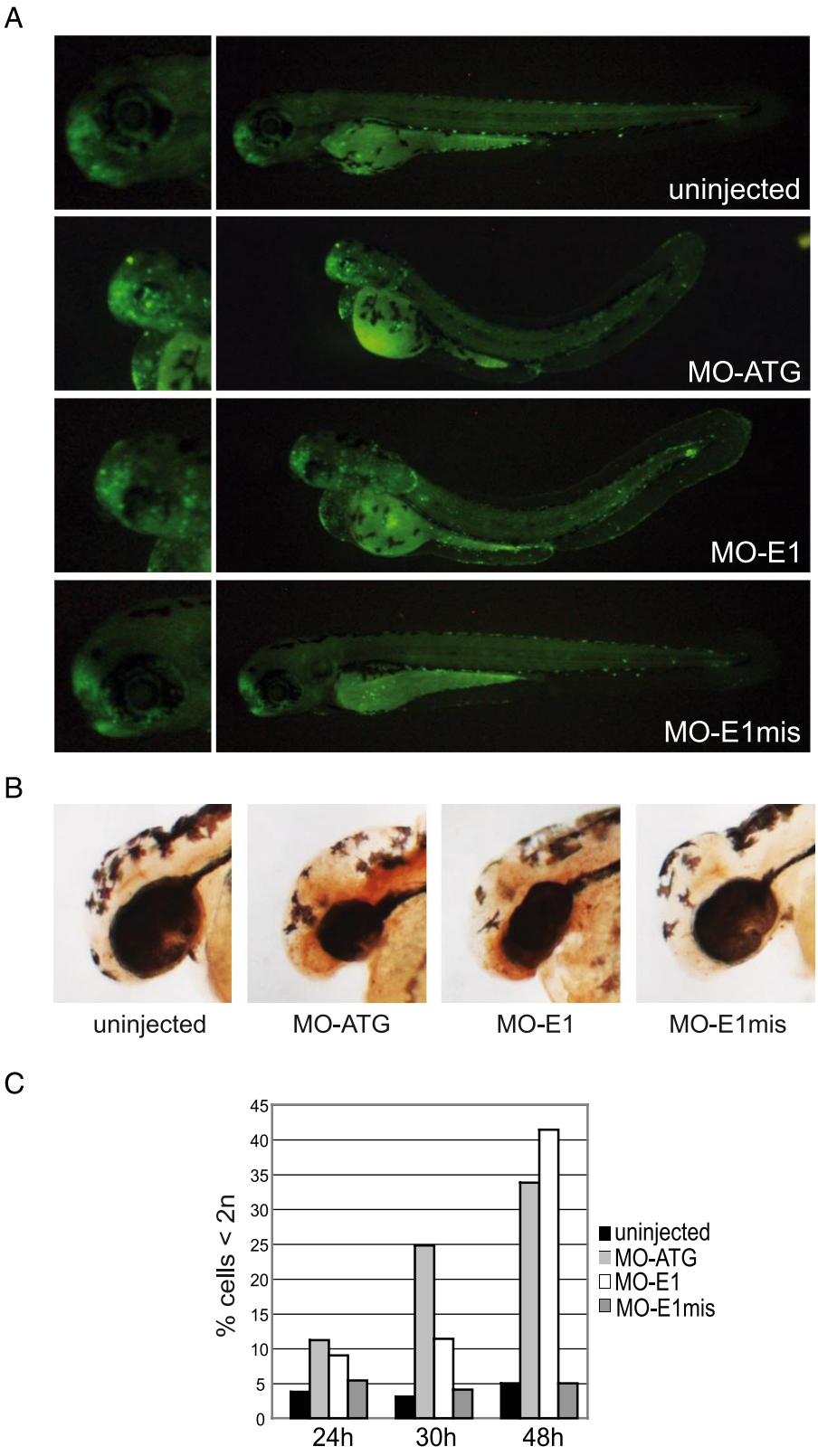

FIGURE 4. **Enhanced apoptosis in *lin9* morphant brains.** *A*, 72 hpf uninjected and morpholino (7 ng)-injected embryos were incubated with the vital dye acridine orange. Fluorescent areas are spread throughout the morphant brains, indicating abnormal apoptosis. *Left*, magnified views of the heads are given. *B*, 48 hpf uninjected and morpholino-injected embryos were paraformaldehyde-fixed, and TUNEL assays where performed. *Brown* 3,3′-diaminobenzidine staining indicates enhanced apoptosis in the brain and olfactory regions of *lin9* morphant embryos. *C*, representative distribution of apoptotic cells in uninjected and morpholino-injected embryos at the indicated hpf. Cells were identified as subdiploid (<*2n*) by flow cytometry.

instance, KIFC1 and KIF11 are kinesins required for proper spindle formation (24, 25), whereas KIF20B/MPP1 and KIF23 exert their function in cytokinesis (26–28). CDC20 and UBCH10 are known regulators of the anaphase-promoting complex (29, 30). CDC14 dephosphorylates securin, which in turn allows the ubiquitination of securin by the anaphase-promoting complex (31). Thus, CDC14 promotes securin destruction and consequently activation of separase, ultimately leading to sister chromatid separation. NUSAP (nucleolar and spindle-associated protein) is ubiquitinated by the anaphase-promoting complex, and its depletion results in aberrant mitotic spindles, defective chromosome segregation, and cytokinesis (32, 33). Recently, Sunkel and co-workers (34) reported that TOP2A positively regulates Aurora B kinase activity, thereby ensuring proper sister chromatid separation. Furthermore, RNA interference-mediated knockdown of TACC3 in HeLa cells results in a reduction of Aurora B kinase and BUBR1 levels at the kinetochores (35). Taken together, the majority of newly identified targets of LIN9 are involved in various mitotic processes, including a preference for the metaphase/anaphase switch.

LIN9 has been reported as a repressor of genes required for G_1/S transition in human cells (5). The fact that *lin9* morphants show a reduced amount of cells in G_1 might point to this repressive function (Fig. 3). However, one would expect an increase in the amount of S phase cells if Lin9 depletion shortens the G_1 phase. Since this is not the case and since we found that *lin9* morphant cells accumulate in mitosis, we assume that the decrease of cell number in G_1 is explained by the increase in G_2/M. Thus, Lin9 is mainly required for mitosis and not the G_1/S phase of the cell cycle. This conclusion is further supported by the fact that we did not identify G_1/S-regulatory genes in our microarray approach (supplemental Fig. 3).

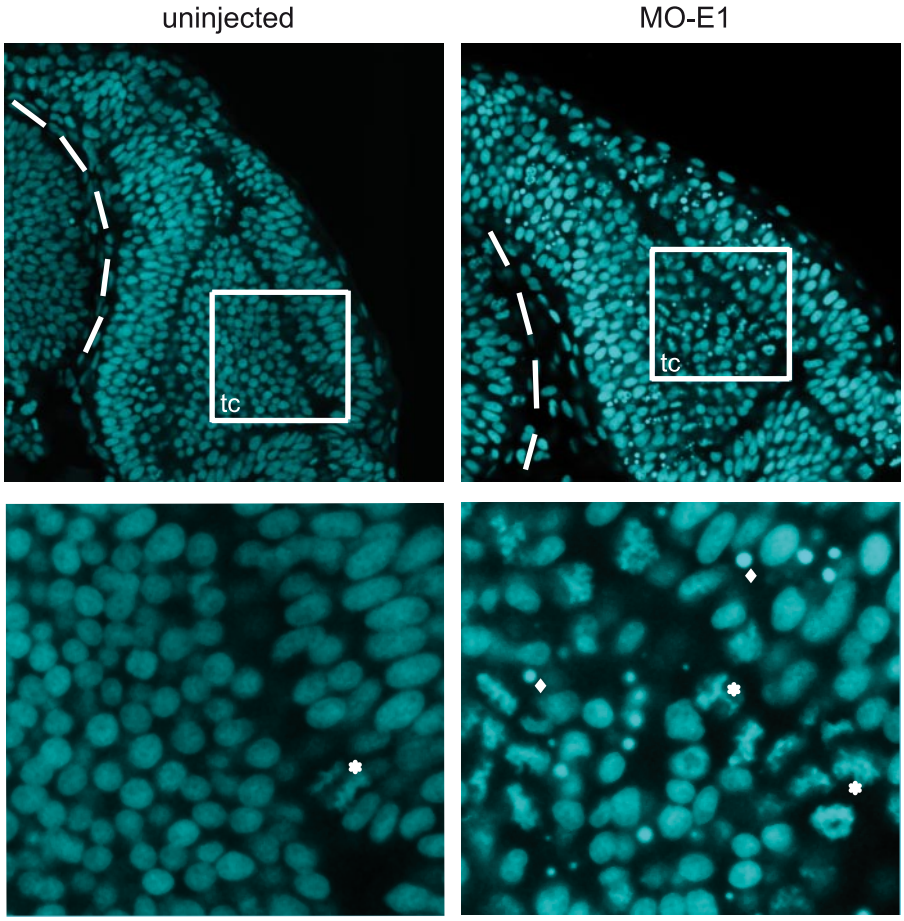

FIGURE 5. **Increase of apoptotic and mitotic cell numbers in the central nervous system of morphant embryos.** Embryos were fixed and Hoechst-stained 30 hpf. Confocal images were taken of the brain (dorsal view). *Dashed lines encircle* the eye. *Below*, magnified views of wild type and E1 morphant optic tectum (*tc*). Examples of mitotic cells (*) and apoptotic bodies (♦) are indicated.

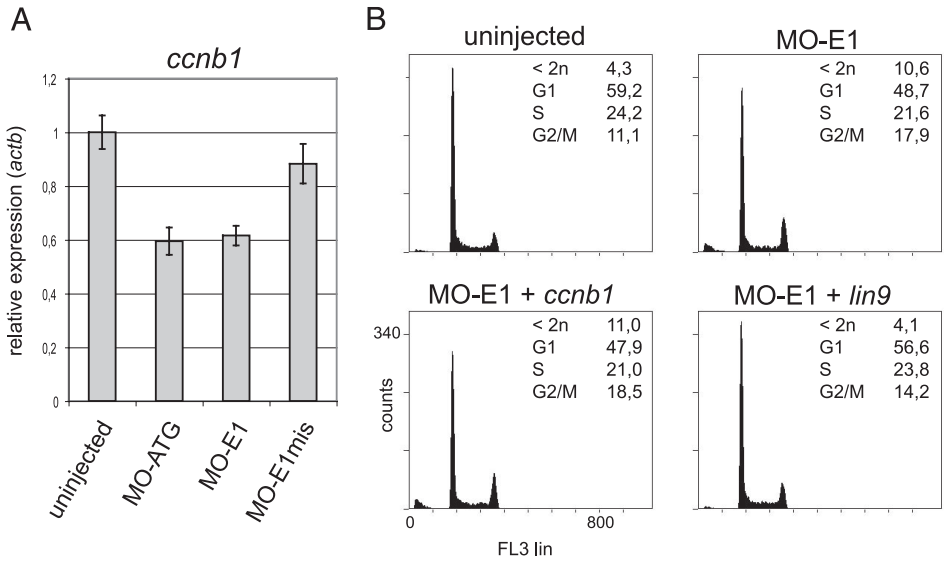

FIGURE 6. **Coinjection of cyclin B (*ccnb1*) mRNA does not rescue cell cycle defects evoked by MO-E1.** *A*, *ccnb1* is down-regulated in *lin9* morphants. Embryos were injected with 7 ng of morpholinos as indicated. 30 hpf *ccnb1* expression was measured by RT-qPCR. *B*, embryos were injected with MO-E1 (7 ng) alone, MO-E1 with *ccnb1* mRNA (0.2 ng), or MO-E1 with LIN9 mRNA (0.2 ng). DNA content was measured by flow cytometry 30 hpf.

The cooperation of LIN9 and B-MYB as members of the LINC/DREAM complex in S phase has been reported for human cells and invertebrate models as well (3, 11). Hence, we expected that both proteins also conjointly regulate cell cycle genes during zebrafish development. Indeed, we find a clear overlap of the *lin9* morphant phenotype with the *bmyb* loss-of-function mutant *crb*. *Aspm*, *cdc2*, *cdc20*, *tacc3*, *kif23*, *kif11*, *anln*, and *oip5* are down-regulated in both *bmyb*- and *lin9*-deficient embryos (15). Furthermore, *crb* embryos display an accumulation of cells in G_2/M, increased apoptosis, and small heads. However, cyclin B mRNA injection partially rescued the *crb* but not the *lin9* morphant phenotype (15). It is thinkable that B-Myb only partially relies on Lin9 in gene activation, and in turn, Lin9 might regulate some G_2/M genes independently of B-Myb. A complete loss-of-function mutation of *lin9* might finally unravel the degree of Lin9 and B-Myb cooperation in zebrafish development.

We found the most striking phenotypic outcome of *lin9* morphants in the central nervous system (*i.e.* an unusually high number of mitotic cells and apoptotic bodies) (Fig. 5 and supplemental Fig. 2). This phenotype is consistent with the expression of *lin9* in zebrafish development. During the pharyngula period (24–48 hpf), the highest *lin9* transcript levels were detected in the optic tectum. Given that the optic tectum represents a highly proliferative area during early stages of zebrafish embryogenesis, we speculate that expression of *lin9* is functionally connected with its requirement in embryonic cell cycle regulation (36, 37).

Cell cycle abnormalities are first detectable at the end of the segmentation period (22–24 h after fertilization) in *lin9* morphants. These effects seem to be relatively late compared with other vertebrates but are not surprising given that the embryo derives an abundant level of maternal factors that ensure development even after the initiation of embryonic gene expression (38). Interestingly, loss-of-function mutations in the majority of essential genes in zebrafish result in cell death of the developing central nervous system, including the Lin9 target genes *kif23*,

A

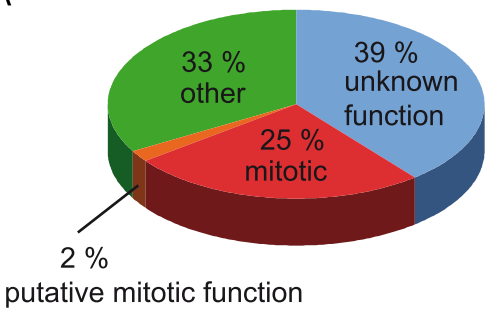

B

entry into mitosis
cks1
cdc2
ccng1
ccnf
plk1

spindle assembly
kifc1
tuba1
kif11
ase1
gpsm2/lgn
tuba8l

centrosomal
aspm
hmmr
odf2/cenexin
plk1

metaphase/anaphase transition
cdc20
ubch10
oip5/mis18beta
cdc14a
plk1
pif1
nusap
top2a
tacc3

cytokinesis
anln/anillin
kif20b/mpp1
kif23

C

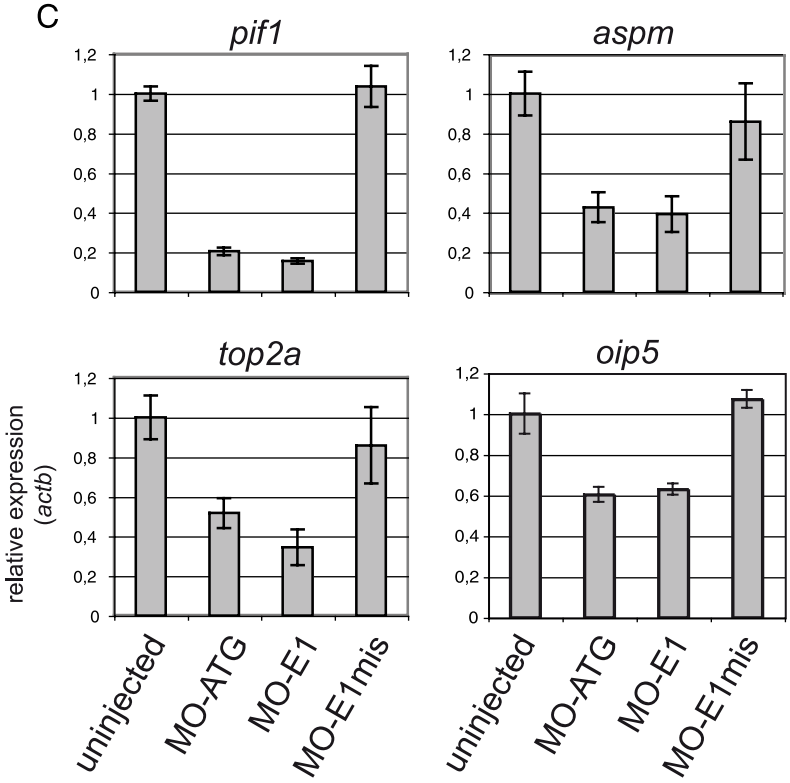

D

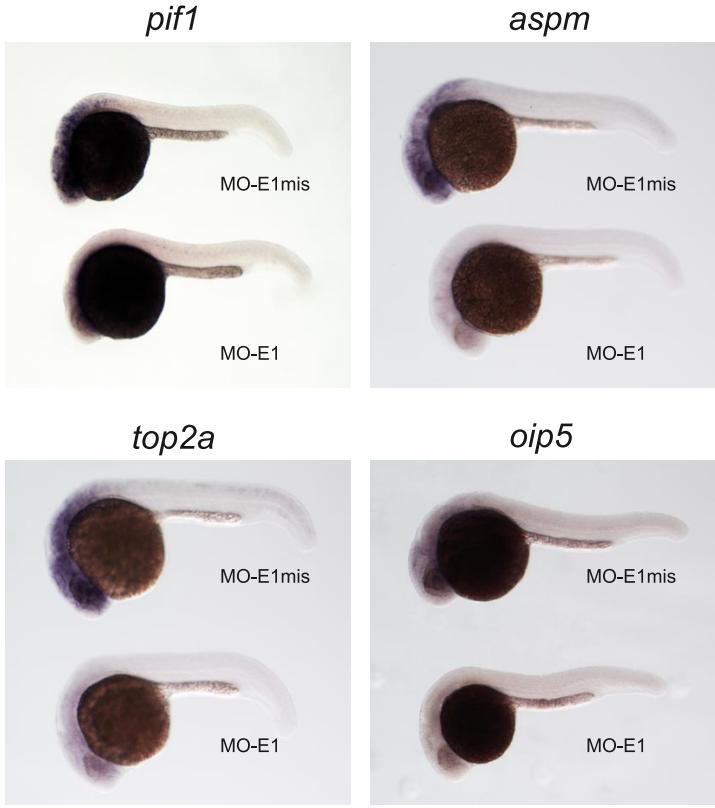

FIGURE 7. **Microarray analysis reveals that mitotic genes are down-regulated in *lin9* morphants.** *A*, functional clustering of genes that are down-regulated ≥1.6-fold in E1 relative to E1mis morphants 24 hpf. *B*, subclassification of LIN9 targets according to their mitotic function. *C*, validation of newly identified LIN9 targets by RT-qPCR. As controls, RNA from uninjected and ATG morphants were included. *D*, whole mount *in situ* hybridization (24 hpf) for *pif1*, *aspm*, *top2a*, and *oip5* on MO-E1- and MO-E1mis-injected embryos.

kif11, *cdc2*, *plk1*, and *top2a* (39). Therefore, *lin9* is essential for embryogenesis, because it activates factors that themselves regulate essential cellular processes.

We do not know when *lin9* morphant cells exit the cell cycle to undergo apoptosis and whether this depends on failures in mitotic progression. However, our flow cytometry data show that the mitotic delay is first detectable shortly before apoptosis arises (data not shown). We therefore speculate that the delay in mitotic progression precedes apoptosis. Clearly, further experiments are necessary to define the pathways that lead to apoptosis upon inhibition of *lin9*.

Acknowledgments—We appreciate the advice of the Schartl group regarding zebrafish care and breeding. We thank Michael Krause and the Genomics Unit of the Institute of Molecular Biology and Tumor Research, Marburg, for gene expression profiling.

REFERENCES

1. Dimova, D. K., and Dyson, N. J. (2005) *Oncogene* **24,** 2810–2826
2. Zhu, W., Giangrande, P. H., and Nevins, J. R. (2004) *EMBO J.* **23,** 4615–4626
3. Osterloh, L., von Eyss, B., Schmit, F., Rein, L., Hubner, D., Samans, B., Hauser, S., and Gaubatz, S. (2007) *EMBO J.* **26,** 144–157
4. Laoukili, J., Kooistra, M. R., Bras, A., Kauw, J., Kerkhoven, R. M., Morrison, A., Clevers, H., and Medema, R. H. (2005) *Nat. Cell Biol.* **7,** 126–136
5. Litovchick, L., Sadasivam, S., Florens, L., Zhu, X., Swanson, S. K., Velmurugan, S., Chen, R., Washburn, M. P., Liu, X. S., and DeCaprio, J. A. (2007) *Mol. Cell* **26,** 539–551
6. Pilkinton, M., Sandoval, R., Song, J., Ness, S. A., and Colamonici, O. R. (2007) *J. Biol. Chem.* **282,** 168–175
7. Schmit, F., Korenjak, M., Mannefeld, M., Schmitt, K., Franke, C., von Eyss, B., Gagrica, S., Hanel, F., Brehm, A., and Gaubatz, S. (2007) *Cell Cycle* **6,** 1903–1913
8. Pilkinton, M., Sandoval, R., and Colamonici, O. R. (2007) *Oncogene* **26,** 7535–7543
9. Lewis, P. W., Beall, E. L., Fleischer, T. C., Georlette, D., Link, A. J., and Botchan, M. R. (2004) *Genes Dev.* **18,** 2929–2940
10. Korenjak, M., Taylor-Harding, B., Binne, U. K., Satterlee, J. S., Stevaux, O., Aasland, R., White-Cooper, H., Dyson, N., and Brehm, A. (2004) *Cell* **119,** 181–193
11. Georlette, D., Ahn, S., MacAlpine, D. M., Cheung, E., Lewis, P. W., Beall, E. L., Bell, S. P., Speed, T., Manak, J. R., and Botchan, M. R. (2007) *Genes Dev.* **21,** 2880–2896
12. Harrison, M. M., Ceol, C. J., Lu, X., and Horvitz, H. R. (2006) *Proc. Natl. Acad. Sci. U. S. A.* **103,** 16782–16787
13. Tanaka, Y., Patestos, N. P., Maekawa, T., and Ishii, S. (1999) *J. Biol. Chem.* **274,** 28067–28070
14. Tarasov, K. V., Tarasova, Y. S., Tam, W. L., Riordon, D. R., Elliott, S. T., Kania, G., Li, J., Yamanaka, S., Crider, D. G., Testa, G., Li, R. A., Lim, B., Stewart, C. L., Liu, Y., Van Eyk, J. E., Wersto, R. P., Wobus, A. M., and Boheler, K. R. (2008) *PLoS ONE* **3,** e2478
15. Shepard, J. L., Amatruda, J. F., Stern, H. M., Subramanian, A., Finkelstein, D., Ziai, J., Finley, K. R., Pfaff, K. L., Hersey, C., Zhou, Y., Barut, B., Freedman, M., Lee, C., Spitsbergen, J., Neuberg, D., Weber, G., Golub, T. R., Glickman, J. N., Kutok, J. L., Aster, J. C., and Zon, L. I. (2005) *Proc. Natl. Acad. Sci. U. S. A.* **102,** 13194–13199
16. Sandoval, R., Xue, J., Tian, X., Barrett, K., Pilkinton, M., Ucker, D. S., Raychaudhuri, P., Kineman, R. D., Luque, R. M., Baida, G., Zou, X., Valli, V. E., Cook, J. L., Kiyokawa, H., and Colamonici, O. R. (2006) *Exp. Cell Res.* **312,** 2465–2475
17. Westerfield, M. (1993) *The Zebrafish Book: A Guide for the Laboratory Use of Zebrafish* (*Brachydanio rerio*), University of Oregon Press, Eugene, OR
18. Kimmel, C. B., Ballard, W. W., Kimmel, S. R., Ullmann, B., and Schilling, T. F. (1995) *Dev. Dyn* **203,** 253–310
19. Pfaffl, M. W. (2001) *Nucleic Acids Res.* **29,** e45
20. Herpin, A., Schindler, D., Kraiss, A., Hornung, U., Winkler, C., and Schartl, M. (2007) *BMC Dev. Biol.* **7,** 99
21. Wagner, T. U., Kraeussling, M., Fedorov, L. M., Reiss, C., Kneitz, B., and Schartl, M. (2009) *Stem Cells Dev.* **18,** 151–160
22. Kleinschmidt, M. A., Streubel, G., Samans, B., Krause, M., and Bauer, U. M. (2008) *Nucleic Acids Res.* **36,** 3202–3213
23. Cole, L. K., and Ross, L. S. (2001) *Dev. Biol.* **240,** 123–142
24. Zhu, C., Zhao, J., Bibikova, M., Leverson, J. D., Bossy-Wetzel, E., Fan, J. B., Abraham, R. T., and Jiang, W. (2005) *Mol. Biol. Cell* **16,** 3187–3199
25. Whitehead, C. M., and Rattner, J. B. (1998) *J. Cell Sci.* **111,** 2551–2561
26. Abaza, A., Soleilhac, J. M., Westendorf, J., Piel, M., Crevel, I., Roux, A., and Pirollet, F. (2003) *J. Biol. Chem.* **278,** 27844–27852
27. Liu, X., Zhou, T., Kuriyama, R., and Erikson, R. L. (2004) *J. Cell Sci.* **117,** 3233–3246
28. Zhu, C., Bossy-Wetzel, E., and Jiang, W. (2005) *Biochem. J.* **389,** 373–381
29. Hwang, L. H., Lau, L. F., Smith, D. L., Mistrot, C. A., Hardwick, K. G., Hwang, E. S., Amon, A., and Murray, A. W. (1998) *Science* **279,** 1041–1044
30. Summers, M. K., Pan, B., Mukhyala, K., and Jackson, P. K. (2008) *Mol. Cell* **31,** 544–556
31. Holt, L. J., Krutchinsky, A. N., and Morgan, D. O. (2008) *Nature* **454,** 353–357
32. Raemaekers, T., Ribbeck, K., Beaudouin, J., Annaert, W., Van Camp, M., Stockmans, I., Smets, N., Bouillon, R., Ellenberg, J., and Carmeliet, G. (2003) *J. Cell Biol.* **162,** 1017–1029
33. Li, L., Zhou, Y., Sun, L., Xing, G., Tian, C., Sun, J., Zhang, L., and He, F. (2007) *Cell. Signal.* **19,** 2046–2055
34. Coelho, P. A., Queiroz-Machado, J., Carmo, A. M., Moutinho-Pereira, S., Maiato, H., and Sunkel, C. E. (2008) *PLoS Biol.* **6,** e207
35. Schneider, L., Essmann, F., Kletke, A., Rio, P., Hanenberg, H., Wetzel, W., Schulze-Osthoff, K., Nurnberg, B., and Piekorz, R. P. (2007) *J. Biol. Chem.* **282,** 29273–29283
36. Wullimann, M. F., and Knipp, S. (2000) *Anat. Embryol.* (*Berl.*) **202,** 385–400
37. Mueller, T., and Wullimann, M. F. (2003) *Brain Res. Dev. Brain Res.* **140,** 137–155
38. Pelegri, F. (2003) *Dev. Dyn.* **228,** 535–554
39. Amsterdam, A., Nissen, R. M., Sun, Z., Swindell, E. C., Farrington, S., and Hopkins, N. (2004) *Proc. Natl. Acad. Sci. U. S. A.* **101,** 12792–12797